HHS Public Access

Author manuscript

Exp Eye Res. Author manuscript; available in PMC 2017 October 01.

Published in final edited form as:

Exp Eye Res. 2016 October ; 151: 68–74. doi:10.1016/j.exer.2016.08.003.

Method for single illumination source combined optical coherence tomography and fluorescence imaging of fluorescently labeled ocular structures in transgenic mice

Ryan P. McNabb[1,*], **Tomas Blanco**[1], **Howard M. Bomze**[1], **Henry C. Tseng**[1], **Daniel R. Saban**[1], **Joseph A. Izatt**[2,1], and **Anthony N. Kuo**[1]

[1]Duke Eye Center and Department of Ophthalmology, Duke University Medical Center, Durham, NC 27710

[2]Department of Biomedical Engineering, Duke University, Durham, NC 27708

Abstract

In vivo imaging permits longitudinal study of ocular disease processes in the same animal over time. Two different *in vivo* optical imaging modalities – optical coherence tomography (OCT) and fluorescence – provide important structural and cellular data respectively about disease processes. In this Methods in Eye Research article, we describe and demonstrate the combination of these two modalities producing a truly simultaneous OCT and fluorescence imaging system for imaging of fluorescently labeled animal models. This system uses only a single light source to illuminate both modalities, and both share the same field of view. This allows simultaneous acquisition of OCT and fluorescence images, and the benefits of both techniques are realized without incurring increased costs in variability, light exposure, time, and post-processing effort as would occur when the modalities are used separately. We then utilized this system to demonstrate multi-modal imaging in a progression of samples exhibiting both fluorescence and OCT scattering beginning with resolution targets, *ex vivo* thy1-YFP labeled neurons in mouse eyes, and finally an *in vivo* longitudinal time course of GFP labelled myeloid cells in a mouse model of ocular allergy.

1. Introduction

Non-destructive *in vivo* imaging permits the longitudinal study of disease processes in the same organism over time. Observing longitudinal changes in the same organism is necessary for understanding the evolution of existing disease processes or for observing chronological changes in age dependent diseases. Two important non-destructive *in vivo* ophthalmic imaging techniques are fluorescence imaging and optical coherence tomography (OCT). Fluorescence imaging is used throughout the biological sciences to selectively image specific processes or cell populations -- such as retinal ganglion cells (RGCs) -- that can then be used to longitudinally study the associated disease processes [1–4]. OCT is a separate non-destructive, *in vivo* imaging modality used in both the basic science and clinical settings. OCT produces label-free, high resolution cross-sectional images to allow

[*]**Corresponding Author:** Ryan P. McNabb, ryan.mcnabb@dm.duke.edu.

Financial Disclosures

detection of changes in ocular microanatomy as a result of disease [5–8]. These two modalities provide complementary types of pathophysiological information – cellular and microanatomical data.

The most straightforward way to gain the benefits of both fluorescence and OCT imaging techniques is to use both modalities one right after the other [4, 9]. This incurs costs such as longer imaging sessions, more animal handling and anesthesia, prolonged light exposure for the animal, and additional post-processing time to register and correlate the fluorescence and OCT images together. In our experience, faster imaging promotes animal health. More recently, in an effort to obtain the advantages of both imaging modalities in a single apparatus and imaging session, a confocal scanning laser ophthalmoscope and OCT system were combined and used to correlate fluorescently labelled RGC loss with retinal anatomical changes over 2 weeks in a N-methyl-D-aspartate induced mouse model of RGC death [9]. However, this system utilized two independent systems with two separate light sources and two differing fields of view acquired simultaneously. Therefore, light exposure was still increased and post processing time was still required for correlation of both imaging modalities.

To achieve truly simultaneous OCT and fluorescence imaging, we have developed a dual modality system that efficiently uses a single illumination source and a single set of optics to obtain identical fields of view for both modalities. Our OCT-fluorescence system uses wavelengths centered at 482nm for the use of imaging transgenic, fluorescent protein expressing mice instead of the infrared light source typical in current commercial OCT systems. A similar system was previously used in the limited application of autofluorescence imaging of lipofuscin within mouse eyes [10]. The use of shorter wavelength light provides two advantages: 1) higher resolution for a given numerical aperture (confocal lateral resolution) and source bandwidth (OCT axial resolution) and 2) the ability to excite common fluorophores such as green and yellow fluorescent proteins (GFP and YFP). This means that as blue light is scanned across the sample, both OCT and fluorescent images are *simultaneously acquired in the exact same location* and are thus automatically spatially registered. This significantly decreases animal handling, anesthesia exposure, and image-processing time because both images are acquired simultaneously. Here we present materials and methods for others to build their own systems to image transgenic mice exhibiting green and yellow fluorescent proteins offering significantly more targets of application.

2. Materials and Supplies

We developed this OCT-fluorescence system utilizing only off-the-shelf parts (Fig. 1). We designed the system to image samples with cells expressing GFP and YFP which have their respective excitation bands at approximately 488nm. Individual filters may be swapped out to image other fluorophores.

2.1 – Materials for Light Source

- Supercontinuum laser emitting desired excitation wavelengths – SuperK EXB-6 or EXW-12, NKT Photonics A/S

- Broadband dielectric mirrors for visible wavelengths – BB1-E02, Thorlabs, Inc.
- Neutral density filter – NDC-50C-4M, Thorlabs, Inc.
- 482nm 25nm bandpass filter – FF01-481/25-25, Semrock, Inc.
- Objective – RMS10X-PF, Thorlabs, Inc.
- 2×2 fused fiber coupler - FC488-50B-APC or FC488-90B-APC, Thorlabs, Inc.

2.2 – Materials for OCT and Fluorescence System

- Reflective fiber collimator – RC02APC-P01, Thorlabs, Inc.
- Fluorescence collection fiber collimation lens – AC254-075-A, Thorlabs, Inc.
- Dichroic mirror – MD498, Thorlabs Inc.
- 525nm 39nm bandpass filter – MF525-39, Thorlabs, Inc.
- 10mm X-Y galvonometer scanning mirror pair – GVS012, Thorlabs, Inc.
- Telecentric imaging lens – V40LC, Volk Optical, Inc.
- Posterior segment imaging diopter control – 2x #63-707, Edmund Optics, Inc.
- Posterior segment imaging optics – 1x #47-711, 1x #47-700, 1x #63-706, Edmund Optics, Inc.
- Multimode fiber – M43L02, Thorlabs, Inc.
- Photomultiplier tube – H7422-40, Hamamatsu Photonics, K.K.

2.3 – Materials for OCT Reference Arm

- Reflective fiber collimator – RC02APC-P01, Thorlabs, Inc.
- Neutral density filter – NDC-50C-4M, Thorlabs, Inc.
- Imaging lens– AC254-050-A, Thorlabs, Inc.
- Protected silver mirror – PF10-03-P01, Thorlabs, Inc.

2.4 – Materials for OCT Spectrometer

- Fiber collimation lens – AL50100-A, Thorlabs, Inc.
- Holographic diffraction grating – WP-1800/532-50.8, Wasatch Photonics, Inc.
- Fold mirror – PF20-03-P01, Thorlabs, Inc.
- Focusing lenses – 2x AC508-500-A, 1x AC508-1000-A, Thorlabs, Inc.
- 1024 pixel line-scan CCD camera – AViiVA SM2, e2v, Inc.

- Calibration Lamp – XE-1, Ocean Optics, Inc.

2.5 – Imaging Samples

- Positive 1951 USAF test chart – #38-257, Edmund Optics, Inc.
- Fluorescent Microbeads – Dragon Green FS06F and FS07F, Bangs Laboratories, Inc.
- thy1-YFP mice – Laboratory of Guo-Ping Feng, PhD (Massachusetts Institute of Technology)
- CX3CR1-GFP knock-in reporter mice – The Jackson Laboratory

3. Detailed Methods

Equations 1–3 [11] describe the resolution considerations when combining OCT and fluorescence detection with a single illumination beam where λ_0 is the center wavelength and $\Delta\lambda$ is the bandwidth of the illumination source. By using optical fiber for both illumination and collection, both techniques were confocally gated. Using the same single-mode fiber for illumination and collection would yield similar lateral and transverse resolutions for both modalities given the numerical aperture of the imaging optics (δx_{FWHM}, see Eq. 1) and differing only due to wavelength [11]. While the single-mode illumination fiber was used for OCT collection, fluorescence collection efficiency was increased with minimal loss in depth sectioning and a slight loss in lateral resolution by utilizing a multimode fiber with a core that was 2–4 times the spot diameter on the fiber [12]. The confocal gates also determined the Rayleigh ranges of the system which corresponded to the depth of field for OCT imaging and axial resolution for fluorescence imaging (δz_F and DOF_{OCT}, see Eq. 2) [11]. Because OCT is an interferometric technique, its axial resolution is independent of the confocal gate and is thus determined not by the imaging optics but by the coherence length of the source which is a function of the center wavelength and bandwidth of the source. Coherence length is typically much smaller than the Rayleigh range (l_c and δz_{OCT}, see Eq. 3) in conventional OCT systems.

$$\delta x_{FWHM} = \frac{1.1603}{\pi}\frac{\lambda_0}{NA} \approx 4.1\mu m \quad (1)$$

$$\delta z_F = DOF_{OCT} = \frac{2\pi\left(0.85\,\delta x_{FWHM}^2\right)}{\lambda_0} \approx 200\mu m \quad (2)$$

$$l_c = \delta z_{OCT} = \frac{2\,ln\,2}{\pi}\frac{\lambda_0^2}{\Delta\lambda} \approx 4.1\mu m \quad (3)$$

We used a supercontinuum laser (EXB-6 or EXW-12, NKT Photonics A/S) which provided a spatially coherent source with low temporal coherence at the excitation wavelengths of GFP and YFP. We filtered infrared light by reflecting the output of the laser from two broadband dielectric mirrors for visible wavelengths (BB1-E02, Thorlabs, Inc.). We further filtered the output of the supercontinuum laser to be centered at 482nm with 25nm bandwidth (FF01-481/25-25, Semrock, Inc.). Using Eq. 2, this provided a theoretical OCT axial resolution of 4.1μm. Light was split to the OCT reference and imaging paths via a 2×2 fiber coupler with design wavelengths at 488±15nm. For the telecentric imaging system we utilized the EXB-6 laser and a 50/50 fiber coupler while with the posterior segment imaging system we utilized the EXW-12 laser and an 80/20 fiber coupler.

For the telecentric imaging system, the collimated illumination light of the sample arm was raster-scanned with a pair of offset X-Y scanning mirrors and an imaging objective with a working distance of 20mm giving the system a theoretical lateral resolution of 4.1μm and depth of focus of 200μm (Eq. 1 and Eq. 3). For the posterior segment imaging system, the collimated illumination light was imaged through a telescope where the first lens was able to be manually translated (Fig. 1) providing defocus correction for individual mice. The light was then raster scanned with a pair of offset X-Y scanning mirrors and imaged through a second telescope to the mouse ocular pupil. The optics of the mouse eye were used to focus light on the retina. The posterior segment imaging optics were chosen to have a theoretical lateral resolution of 4.8μm and a depth of focus 250μm. All volumes shown are 500×500×512 pixels (WxLxD) with physical dimensions indicated in each associated image. Since only a fraction of the illumination light would induce fluorescence, we designed a fluorescence detection system that was independent of the OCT channel to efficiently collect and detect the fluorescent signal. Returning fluorescent light was separated via a dichroic mirror (MD498, Thorlabs Inc.), passed through a band-pass dielectric filter (MF525-39, Thorlabs, Inc.), collected by a multimode fiber and detected by a photomultiplier tube (H7422-40, Hamamatsu Photonics, K.K.). For OCT, light backscattered from the sample returned along the illumination path. The backscattered light then mixed with light returning from the OCT reference arm, and the resulting interferogram was detected by a spectrometer.

We chose a spectrometer based system (spectral-domain OCT: SDOCT) to provide flexibility in imaging wavelengths, speed, and range. We designed the spectrometer to be centered at 482nm with a 30nm spread over a 1024 pixel line-scan CCD camera (AViiVA SM2, e2v, Inc.). Given Eq. 4 (where N is number of line-scan camera pixels), this yields a theoretical imaging range of 1.8mm [13]. We designed the optics of the spectrometer such that 90% of the ensquared energy of a given spot fell within the area of the 14μm square pixels of the camera across the entire width of the camera. Table 1 provides spacing and orientation of optics to build the designed spectrometer. All OCT imaging was performed at 10000 A-scans/sec.

$$\Delta D_{OCTSpectrometer} = \frac{N}{4}\frac{\lambda_0^2}{\Delta\lambda} \approx 1.8mm \quad (4)$$

The spectrometer that we designed may be built using the optics listed within Section 2: Materials and Supplies and the prescription listed within Table 1. All lenses in this system are stock lenses however we list the radii of curvature to indicate orientation of lenses within the system. Spectrometer system performance is dependent upon these orientations. We performed calibration of the spectrometer utilizing the emission lines from a xenon calibration lamp (XE-1, Ocean Optics, Inc.). Calibration of the spectrometer is required to accurately resample the detected spectrum from being linear in wavelength to be linear in wavenumber.

To evaluate imaging performance, we imaged a sequence of targets including phantoms for characterization, *ex vivo* imaging of mouse cornea and retina, and *in vivo* imaging of mouse cornea over a week-long longitudinal course. All animals were imaged under IACUC approved protocols. Light on the sample utilizing the telecentric imaging optics was measured to be 600 μW and light prior to the mouse eye utilizing the posterior segment imaging optics was measured to be 250 μW. Both were in accordance with the ANSI standards for human ocular exposure [14, 15]. The non-biological phantoms included a 1951 USAF test chart and fluorescent micro-beads. A chrome-on-glass 1951 USAF test chart was coated over with fluorescent paint such that the chrome was between the glass and fluorescent material. When imaged through the back of the test chart, both chrome and fluorescent material were visible. This allowed for the lateral resolutions of both the OCT and fluorescence channels to be individually and simultaneously measured. Fluorescent beads with an excitation peak at 480nm and an emission peak at 520nm (both similar to GFP and YFP) were used.

To evaluate imaging performance, we imaged a sequence of targets including phantoms for characterization, *ex vivo* imaging of mouse cornea and retina, and *in vivo* imaging of mouse cornea over a week-long longitudinal course. All animals were imaged under IACUC approved protocols. Light on the sample utilizing the telecentric imaging optics was measured to be 600 μW and light prior to the mouse eye utilizing the posterior segment imaging optics was measured to be 250 μW. Both were in accordance with the ANSI standards for human ocular exposure [14, 15]. The non-biological phantoms included a 1951 USAF test chart and fluorescent micro-beads. A chrome-on-glass 1951 USAF test chart was coated over with fluorescent paint such that the chrome was between the glass and fluorescent material. When imaged through the back of the test chart, both chrome and fluorescent material were visible. This allowed for the lateral resolutions of both the OCT and fluorescence channels to be individually and simultaneously measured. Fluorescent beads with an excitation peak at 480nm and an emission peak at 520nm (both similar to GFP and YFP) were used.

For our *ex vivo* imaging study, we used thy1-YFP mice where the thy1 promoter limits expression of YFP to neurons [16] such as retinal ganglion cells and corneal nerves in our eye samples. These ocular neurons are involved in glaucoma and corneal diseases. All *ex vivo* imaging was performed within an hour of sacrifice of the animal, and the retinas were surgically dissected and flat mounted without fixation before being imaged. For *in vivo* anterior segment imaging, we imaged CX3CR1-GFP knock-in reporter mice used as a model for ocular allergy [17, 18]. CX3CR1-GFP specifically labels bone marrow derived

myeloid (monocyte/macrophage) cells involved in the allergic response. These mice were sensitized with ovalbumin (OVA)/pertussis toxin/alum two weeks prior to being challenged with OVA eye drops daily for 6 days to elicit an allergic response. The mice were anesthetized and imaged immediately before and after administration of OVA. For *in vivo* posterior segment imaging, we utilized the same thy1-YFP strain of mice [16] as was used for *ex vivo* imaging. The mice were anesthetized, pupils dilated (0.5% tropicamide + 5% phenylephrine) and immediately imaged.

Figure 2 shows results from imaging the fluorescent-backed 1951 USAF test chart and fluorescent beads which allowed direct measurement of the lateral resolution of both imaging modalities. OCT summed volume projections (SVP) are generated by taking an en face view of an OCT volume and creating an averaged projection of that view. In Fig. 2A, group 6 element 6 (bar width is equal to 4.4μm) is resolvable, validating our optical design. In Fig. 2B, individual 7 μm diameter fluorescent beads are resolvable. A one-to-one correspondence between the OCT and the fluorescence images are shown with no post-processing registration performed. Slight mismatch at the image periphery is due to chromatic aberration imparted by the imaging lens.

Ex vivo cornea and retina from two different thy1-YFP mice are shown in Fig. 3. The OCT B-scans show ocular cross-sectional structure. The corresponding *en face* fluorescence images provide complementary information unseen by OCT alone about cells and nerve axons within the structure. The blue bar within the fluorescence images indicates the location of the displayed OCT B-scan. In the retina image pair, the ganglion cell complex layer (retinal nerve fiber layer, ganglion cell layer, and inner plexiform layer) is distinct in the OCT (left, red arrow). The presence of RGCs and their axons are clearly visualized in the fluorescence image (right). The fluorescent round dots are RGC cell bodies while the curvilinear fluorescent lines are RGC axons as they travel from peripheral retina to the optic nerve to exit the retina (upper right hand corner). All of these structures (ganglion cell complex layer, RGC cells and axons) are important in studying neurodegenerative diseases such as glaucoma. Dark areas (asterisks) are cuts in the tissue for flat-mounting the retina and corresponds to the lack of retinal tissue in the OCT image (asterisks).

In vivo imaging of the CX3CR1-GFP mouse corneas took place over a week. Viewing the entire time course from a representative mouse (Fig. 4), the fluorescent images demonstrate the initial presence of myeloid cells within the cornea on day 0 prior to OVA challenge. As time progressed, the myeloid density within the central region of the cornea increased and peaked on Day 6. Despite the increasing myeloid density and inflammatory response, the cornea showed no gross structural changes on OCT (i.e. no corneal opacification or bullae) and appeared similar throughout the time course.

In vivo imaging of thy1-YFP mouse retina (shown in Fig.5) was performed utilizing the posterior segment imaging optics with the SuperK EXW-12 laser and the 90/10 2×2 fiber coupler. The system acquired the full 900μm of imaging depth described above however images in Fig. 5 only show the relevant 450μm of depth that contained retina. Both OCT volumes and repeated B-scans were acquired. Twenty five repeated B-scans were registered and averaged to create the B-scan shown in Fig. 5A. Figures 5B and 5C show the OCT SVP

and fluorescence images respectively from a single volume acquisition. Figure 5D shows the complete OCT volume rendered using enhanced ray-casting [19] and the location of the B-scan shown in Fig. 5A.

4. Pitfalls and Troubleshooting

Conventional multi-modality systems require multiple sources which increase complexity of the system [4, 9, 20, 21]. Additionally both sources contribute to the ocular maximum permissible exposure (MPE) [14, 15]. By utilizing a single source, the full MPE can be devoted to the fluorescence excitation wavelengths to improve fluorescence imaging. Light that does not undergo fluorescence but is instead backscattered may be collected and utilized for OCT imaging. Thus, this system more efficiently uses light that interacts with the sample. This has the added benefit of ensuring that the light detected by both the SDOCT spectrometer and the fluorescence PMT came from the same illumination confocal gate and providing automatic co-registration of both. There are currently available commercial systems exist that provide simultaneous OCT and fluorescence images but suffer from the problems described above including the requirement for multiple sources as well as other limitations. The Micron Phoenix IV [22] combines a separate OCT system with a wide-field illumination fluorescence imaging system. While the OCT imaging system employs a confocal gate, the fluorescence channel does not due to the wide-field illumination schema utilized. Practically what this means is that any part of the cornea or lens that exhibit fluorescence will contribute signal to a retinal image and conversely any retinal structures that exhibit fluorescence will contribute signal to a corneal or lens image adding unwanted background noise and potentially washing out the desired fluorescent signal. The Heidelberg Spectralis HRT+OCT [24] combines OCT with a separate blue wavelength scanning laser ophthalmoscope (SLO) where each utilizes a separate confocal gate. However this system requires multiple sources that contribute to the ocular MPE and more importantly is designed primarily for imaging human subjects.

There are limitations for this system when compared to other dedicated OCT or fluorescence imaging systems. A primary limitation for the OCT collection is that it must occur at the fluorescence excitation wavelength. If different excitation wavelengths are desired for other fluorophores, the SDOCT spectrometer would need to be redesigned and realigned. An additional effect of OCT imaging at 482nm is the greater absorption of melanin and increased scattering within tissue versus imaging within the near-infrared [24]. A dual modality imaging system based on a frequency doubled Ti:Sapphire laser, such as [25] where the center wavelength was 415nm, would be further limited by melanin absorption and would lack the ability to image GFP or YFP. For the fluorescence imaging, the primary limitation is the lack of fine depth sectioning with this design. The long confocal gate required for SDOCT imaging currently limits fluorescence imaging to a single coincident *en face* image. A system that combines two-photon microscopy with OCT has been shown which allows for fluorescence depth-sectioning but is limited thus far to *ex vivo* imaging due to the light intensity used [26].

Future versions of this system could potentially address currently present shortfalls, particularly in regards to fluorescence imaging. Currently, the fluorescence channel has a

limited dynamic range and appears over exposed in both the *ex vivo* and *in vivo* thy1-YFP retinal images, particularly near the optic nerve head. A larger dynamic range may allow for improved visualization of the nerve fiber layer near the nerve head in these mice. Additionally, the current version of the system provides only qualitative information about location of fluorescence excitation. Quantitative information about the fluorescence intensity could potentially be obtained through careful calibration possibly with the use of a NIST fluorescence standard. Calibration could enable longitudinal studies examining the exhibited cellular fluorescence intensity in a quantitative manner. To expand upon this, due to the simultaneously acquired and co-located OCT structural information, one could potentially obtain improved registration of images that account for tissue topography and provide a more accurate way to track a field of cells over time in addition to larger morphological changes.

In conclusion, we have developed a single source simultaneous OCT and fluorescence imaging system and demonstrated imaging in transgenic mice expressing fluorescent proteins. This imaging system has the potential to be a powerful tool for scientists to non-destructively acquire *in* vivo imaging of both structural (OCT) and cellular (fluorescence) changes in disease.

Acknowledgments

We acknowledge financial support from the NIH (R21-EY025427, R01-EY023039, K08-EY021520, P30-EY005722), The Coulter Foundation, and Research to Prevent Blindness.

We would like to acknowledge the assistance of Zachary Johnson, Prithu Mettu MD, and Michael Allingham MD, PhD with the mice used for *in vivo* retinal imaging.

References

1. Higashide T, Kawaguchi I, Ohkubo S, Takeda H, Sugiyama K. In Vivo Imaging and Counting of Rat Retinal Ganglion Cells Using a Scanning Laser Ophthalmoscope. Investigative Ophthalmology & Visual Science. 2006; 47:2943–2950. [PubMed: 16799037]
2. Leung CKS, Lindsey JD, Crowston JG, Ju W-K, Liu Q, Bartsch D-U, Weinreb RN. In vivo imaging of murine retinal ganglion cells. Journal of Neuroscience Methods. 2008; 168:475–478. [PubMed: 18079000]
3. Walsh MK, Quigley HA. In vivo time-lapse fluorescence imaging of individual retinal ganglion cells in mice. Journal of Neuroscience Methods. 2008; 169:214–221. [PubMed: 18199485]
4. Chauhan BC, Stevens KT, Levesque JM, Nuschke AC, Sharpe GP, O'Leary N, Archibald ML, Wang X. Longitudinal In Vivo Imaging of Retinal Ganglion Cells and Retinal Thickness Changes Following Optic Nerve Injury in Mice. PLoS ONE. 2012; 7:e40352. [PubMed: 22768284]
5. Schuman JS, Hee MR, Arya AV, Pedut-Kloizman T, Puliafito CA, Fujimoto JG, Swanson EA. Optical coherence tomography: A new tool for glaucoma diagnosis. Current Opinion in Ophthalmology. 1995; 6:89–95. [PubMed: 10150863]
6. Bowd C, Weinreb RN, Williams JM, Zangwill LM. THe retinal nerve fiber layer thickness in ocular hypertensive, normal, and glaucomatous eyes with optical coherence tomography. Archives of Ophthalmology. 2000; 118:22–26. [PubMed: 10636409]
7. Budenz DL, Anderson DR, Varma R, Schuman J, Cantor L, Savell J, Greenfield DS, Patella VM, Quigley HA, Tielsch J. Determinants of Normal Retinal Nerve Fiber Layer Thickness Measured by Stratus OCT. Ophthalmology. 2007; 114:1046–1052. [PubMed: 17210181]

8. Konstantopoulos A, Yadegarfar G, Fievez M, Anderson DF, Hossain P. In Vivo Quantification of Bacterial Keratitis with Optical Coherence Tomography. Investigative Ophthalmology & Visual Science. 2011; 52:1093–1097. [PubMed: 20926816]
9. Nakano N, Ikeda HO, Hangai M, Muraoka Y, Toda Y, Kakizuka A, Yoshimura N. Longitudinal and Simultaneous Imaging of Retinal Ganglion Cells and Inner Retinal Layers in a Mouse Model of Glaucoma Induced by N-Methyl-d-Aspartate. Investigative Ophthalmology & Visual Science. 2011; 52:8754–8762. [PubMed: 22003119]
10. Jiang, Minshan; Liu, Tan; Liu, Xiaojing; Jiao, Shuliang. Simultaneous optical coherence tomography and lipofuscin autofluorescence imaging of the retina with a single broadband light source at 480nm. Biomed. Opt. Express. 2014; 5:4242–4248. [PubMed: 25574436]
11. Izatt, JA.; Choma, MA. Theory of Optical Coherence Tomography. In: Drexler, W.; Fujimoto, J., editors. Optical Coherence Tomography. Springer Berlin Heidelberg; 2008. p. 47-72.
12. Wilson T, Carlini AR. Size of the detector in confocal imaging systems. Optics Letters. 1987; 12:227–229. [PubMed: 19738847]
13. Hu, Z.; Rollins, AM. Optical Design for OCT. In: Drexler, W.; Fujimoto, J., editors. Optical Coherence Tomography. Springer Berlin Heidelberg; 2008. p. 379-404.
14. ANSI. Z136.1-2007. 2007. Safe Use of Lasers.
15. Delori FC, Webb RH, Sliney DH. Maximum permissible exposures for ocular safety (ANSI 2000), with emphasis on ophthalmic devices. Journal of the Optical Society of America A. 2007; 24:1250–1265.
16. Feng G, Mellor RH, Bernstein M, Keller-Peck C, Nguyen QT, Wallace M, Nerbonne JM, Lichtman JW, Sanes JR. Imaging Neuronal Subsets in Transgenic Mice Expressing Multiple Spectral Variants of GFP. Neuron. 2000; 28:41–51. [PubMed: 11086982]
17. Jung S, Aliberti J, Graemmel P, Sunshine MJ, Kreutzberg GW, Sher A, Littman DR. Analysis of Fractalkine Receptor CX3CR1 Function by Targeted Deletion and Green Fluorescent Protein Reporter Gene Insertion. Molecular and Cellular Biology. 2000; 20:4106–4114. [PubMed: 10805752]
18. Schlereth S, Lee HS, Khandelwal P, Saban DR. Blocking CCR7 at the Ocular Surface Impairs the Pathogenic Contribution of Dendritic Cells in Allergic Conjunctivitis. The American Journal of Pathology. 2012; 180:2351–2360. [PubMed: 22507838]
19. Viehland C, Keller B, Carrasco-Zevallos OM, Nankivil D, Shen L, Mangalesh S, Viet DT, Kuo AN, Toth CA, Izatt JA. Enhanced volumetric visualization for real time 4D intraoperative ophthalmic swept-source OCT. Biomedical Optics Express. 2016; 7:1815–1829. [PubMed: 27231623]
20. Rao KD, Choma MA, Yazdanfar S, Rollins AM, Izatt JA. Molecular contrast in optical coherence tomography by use of a pump probe technique. Optics Letters. 2003; 28:340–342. [PubMed: 12659437]
21. Pahlevaninezhad H, Lee AMD, Shaipanich T, Raizada R, Cahill L, Hohert G, Yang VXD, Lam S, MacAulay C, Lane P. A high-efficiency fiber-based imaging system for co-registered autofluorescence and optical coherence tomography. Biomedical Optics Express. 2014; 5:2978–2987. [PubMed: 25401011]
22. [Accessed June 9, 2016] Mircon Phoenix IV. Retrieved from: http://www.phoenixreslabs.com/products/micron-iv-retinal-imaging-microscope/
23. [Accessed June 9, 2016] Heidelberg Spectralis HRT+OCT. Retrieved from: https://www.heidelbergengineering.com/us/products/spectralis-models/
24. Anderson RR, Parrish JA. The Optics of Human Skin. J Investig Dermatol. 1981; 77:13–19. [PubMed: 7252245]
25. Dai C, Liu X, Jiao S. Simultaneous optical coherence tomography and autofluorescence microscopy with a single light source. Journal of Biomedical Optics. 2012; 17:0805021–0805023.
26. Chong SP, Lai T, Zhou Y, Tang S. Tri-modal microscopy with multiphoton and optical coherence microscopy/tomography for multi-scale and multi-contrast imaging. Biomedical Optics Express. 2013; 4:1584–1594. [PubMed: 24049679]

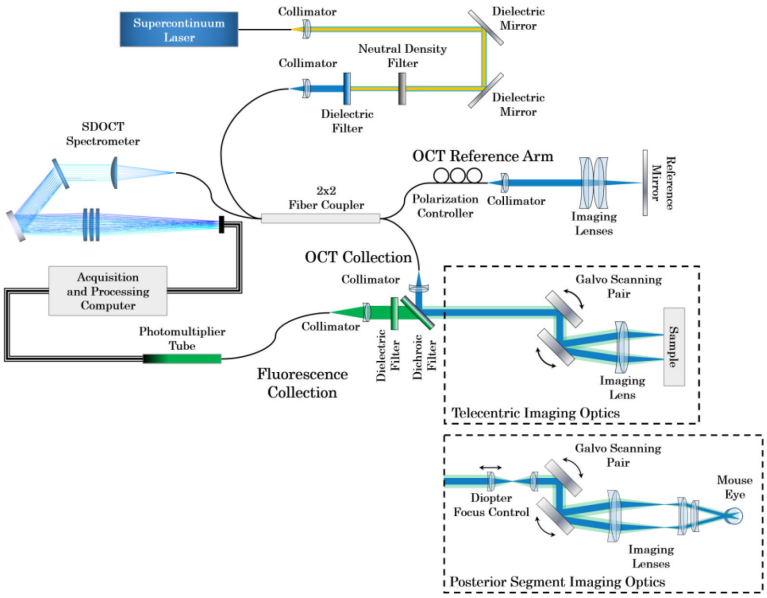

Figure 1.

OCT-fluorescence imaging system schematic. Illumination and backscattered light is in blue. Fluorescence emission is shown in green. Telecentric imaging optics were used for imaging phantoms, *ex vivo* murine anterior segment and retina, and *in vivo* murine anterior segment. Posterior Segment imaging optics were used for imaging *in vivo* murine retina.

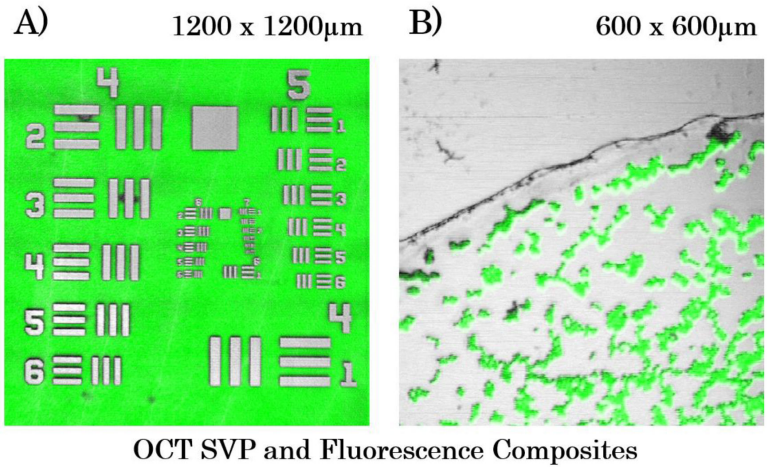

Figure 2.

OCT summed volume projection (SVP; gray scale) and fluorescence (green) composite images *A)* 1951 USAF test chart *B)* Slide mounted 7µm fluorescent beads

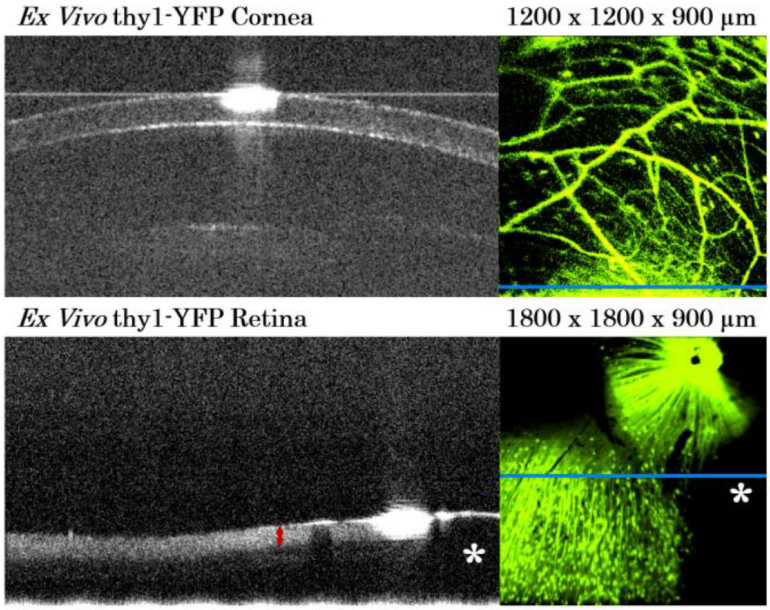

Figure 3.

OCT-fluorescence imaging of *ex vivo* thy1-YFP mouse cornea (*top*) and retina (*bottom*). *Left)* single representative OCT B-scan *Right)* simultaneously acquired fluorescence image showing fluorescently labelled neurons.

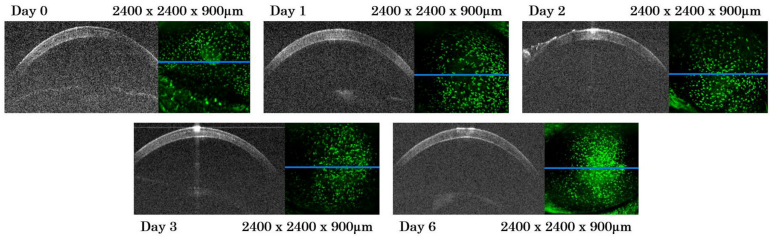

Figure 4.

Longitudinal *in vivo* blue OCT-fluorescence imaging of ocular inflammation in CX3CR1-GFP mouse over one week. For each day, a single OCT B-scan from each volume is on the left, and the simultaneously acquired fluorescence image is on the right. Extraneous structure seen on left side of cornea in day 2 is hydrating gel used to protect the mouse cornea during anesthesia and imaging. The green dots are GFP labeled myeloid cells.

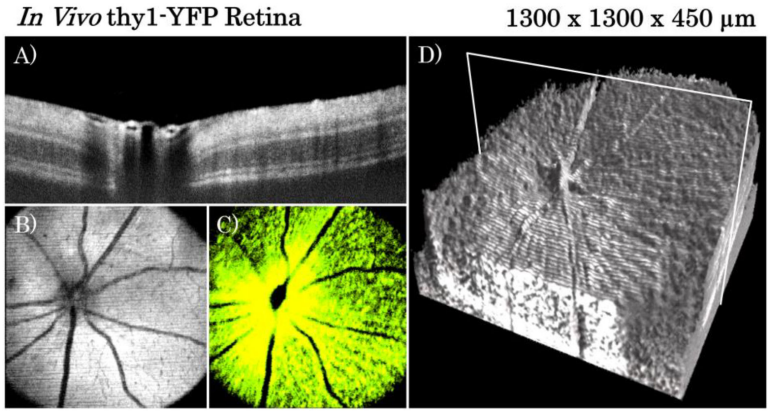

Figure 5.

I*n vivo* blue OCT-fluorescence imaging of thy1-YFP mouse retina. *A)* Averaged repeated B-scans of *in vivo* retina located at the position indicated by the white box in the volume rendering of Fig. 5D. Strong shadows can be seen below blood vessel lumen due to high absorption and scattering by red blood cells at blue wavelengths *B) En face* SVP from OCT volume *C)* Corresponding *en face* fluorescence image *D)* Volumetric rendering of OCT volume data.

Table 1

Prescription for 482nm centered OCT spectrometer

Component	Radius Of Curvature (mm)	Air spacing (mm)	Tilt (degrees)
Fiber			
		91.312	
AL50100-A, Front	Infinity		
AL50100-A, Back	51.12		
		75	25.71
WP-1800/532-50.8			
		70	
PF20-03-P01			
		130	−25.71
AC508-500-A, Front	272.90		
AC508-500-A, Back	970.00		
		3	
AC508-500-A, Front	272.90		
AC508-500-A, Back	970.00		
		3	
AC508-1000-A, Front	738.50		
AC508-1000-A, Back	1023.30		
		190.27	−7.92
AViiVA SM2			